



ELSEVIER

Contents lists available at ScienceDirect

## Chemical Engineering Science

journal homepage: [www.elsevier.com/locate/ces](http://www.elsevier.com/locate/ces)

## Contribution of synchrotron X-ray holotomography to the understanding of liquid distribution in a medium during liquid aerosol filtration

A. Charvet<sup>a,\*</sup>, S. Rolland Du Roscoat<sup>b,c</sup>, M. Peralba<sup>a</sup>, J.F. Bloch<sup>a</sup>, Y. Gonthier<sup>d</sup>

<sup>a</sup> Laboratoire Génie des Procédés Papetiers (LGP2), CNRS UMR 5518, Grenoble-INP Pagora, 461 rue de la Papeterie BP 65, 38402 Saint-Martin-d'Hères Cedex, France

<sup>b</sup> Laboratoire Sols-Solides-Structures-Risques (3S-R), CNRS-UJF-INPG UMR 5521, Domaine Universitaire, BP 53, 38041 Grenoble Cedex 9, France

<sup>c</sup> European Synchrotron Radiation Facility, Polygone Scientifique Louis Néel, 6 rue Jules Horowitz, 38000 Grenoble, France

<sup>d</sup> Laboratoire Optimisation de la Conception et Ingénierie de l'Environnement (LOCIE), CNRS FRE 3220, Université de Savoie, Polytech'Savoie, 73376 Le Bourget du Lac, France

### ARTICLE INFO

#### Article history:

Received 9 July 2010

Received in revised form

13 October 2010

Accepted 3 November 2010

Available online 10 November 2010

#### Keywords:

Aerosol

Filtration

Tomography

Imaging

Porous media

Liquid distribution

### ABSTRACT

The three-dimensional structure of a fibrous filter determines its behaviour during filtration, such as the obtained pressure drop, the fractional efficiency and the filter lifetime. Therefore, suitable parameters describing the inner structure (the local packing density) are key inputs for modelling filter performance accurately. The synchrotron X-ray holotomography, carried out at the European Synchrotron Radiation Facility, was performed in this study to provide information on the three-dimensional structure of a fibrous filter. Moreover, this non-invasive technique was used to determine the liquid distribution in a filter clogged with a liquid aerosol of di-ethyl-hexyl-sebacate. These samples were imaged at a voxel size of 0.7  $\mu\text{m}$ , which allows the quantification of the different phases within the filter (liquid, fibres and void space). The results complete the two-dimensional studies obtained by scanning electron microscopic and highlight the formation of liquid menisci not only on the filter surface but also in the filter depth. Image analyses of synchrotron X-ray holotomography radiographs also highlight a heterogeneous liquid distribution along the thickness of the clogged filter.

© 2010 Elsevier Ltd. All rights reserved.

### 1. Introduction

In recent years, air quality has become a political, scientific and public health issue. Aerosols constitute a significant part of air pollution, but unlike other air contaminants, they are not a well-defined chemical entity but rather a heterogeneous mixture in which each element is characterized by a state (liquid or solid), a particle size distribution and a chemical composition. Mist aerosol particles can be generated in several industrial machining processes by different mechanisms (Boundy et al., 2000; Cooper and Leith, 1998; Gunter and Sutherland, 1999; Simpson et al., 2000). Among these mechanisms, Thornburg and Leith (2000) showed that evaporation–condensation phenomena generated smaller particles (between 0.5 and 3  $\mu\text{m}$ ) than centrifugal force (between 5 and 110  $\mu\text{m}$  depending on the oil type, the rotational speed and the liquid flow). Moreover, liquid aerosols can be generated during the production of compressed gases, which are widely used in industry and laboratories. Oil or water mists in compressed air can induce many problems such as freezing of air lines in cold weather, fouling of instruments, decreasing desiccant efficiency and life

span, rusting of air tools or contamination of air (Brink et al., 1966). These problems result in increased operating and maintenance costs, process down-time and poor product quality.

Among all treatment processes used to prevent problems related to liquid aerosols, fibrous filters are most frequently used to separate particles from airflow. The need to protect both manufacturing processes and people has stimulated both theoretical and experimental research on liquid aerosol filtration. However, the main problem in designing filtration processes is to determine or predict the aging of filters, which is more complicated for the filtration of liquid aerosol than for filtration dedicated to solid aerosol because the trapped fluid is likely to move within the medium. Namely, the pressure drop increase of a fibrous filter clogged with a liquid aerosol is quite different from the pressure drop increase obtained with a solid aerosol. During liquid aerosol filtration, a drainage state occurs, which is characterized by a constant pressure drop. This process does not require any filter regeneration and the two characteristics of filtration of liquid aerosol (drainage and constant pressure drop) suggest that the filters used have an infinite lifetime. This vision is utopian since a liquid aerosol still contains some solid particles, which will degrade and clog the filter. Nevertheless, the use of fibrous filters can still be highly valuable for manufacturers confronted to liquid aerosols and wishing to recover or recycle this liquid. Various authors have studied the clogging of a fibrous filter with a liquid aerosol (di-ethyl-hexyl-sebacate (DEHS), di-octyl-phthalate (DOP) and glycerol) and

\* Corresponding author. Tel.: +33 0 3 83 17 53 33.

E-mail address: [augustin.charvet@ensic.inpl-nancy.fr](mailto:augustin.charvet@ensic.inpl-nancy.fr) (A. Charvet).

<sup>1</sup> Present address: Laboratoire Réactions et Génie des Procédés (LRGP), CNRS UPR 3349, 1 rue Grandville BP 20451, 54001 Nancy Cedex, France.

described how the pressure drop evolved in different stages (Charvet et al., 2008; Contal et al., 2004; Gougeon, 1994; Walsh et al., 1996).

During the first filtration stage, Walsh et al. (1996) reported few differences with solid particle filtration. Indeed, liquid particle capture is located on the fibre surface and the liquid deposit occurs in the form of droplets surrounding the fibres (Fig. 1A). Gougeon (1994) noted that the pressure drop seems to be proportional to the collected liquid mass and increases slowly because the liquid located on the fibre surface does not interfere with flow in the medium. Nevertheless, this deposit produces a slight pressure drop increase due to an increase in packing density (fibrous volume fraction). Tekasakul et al. (2008) also observed that the pressure drop is linearly related to the collected mass.

Gougeon (1994) showed that the second stage begins when a critical trapped mass was reached and an exponential increase in the pressure drop was observed. Agranovski and Braddock (1998) showed that the droplets grow by coalescing with new drops collected and thus cover the fibres. According to Frising et al. (2005), these droplets form a liquid tube around the fibres, increasing their diameter. This liquid tube increases to a maximum diameter, which can vary depending on many parameters such as liquid–fibre surface tension, liquid viscosity or liquid density. However, this assumption is open to criticism. Indeed, Mullins and Kasper (2006) experimentally and theoretically demonstrated that a liquid film without regularly spaced droplets can rarely exist on a single filter fibre because it is broken into distinct droplets by Plateau–Rayleigh instabilities. According to these authors, liquid forms droplets on the fibre surface at their intersections. Liew and Conder (1985) explained the exponential increase in pressure drop by the formation of liquid bridges and films between fibres and at their intersections (Fig. 1B). This was also observed by Frising et al. (2005) and Contal et al. (2004). This clogging of the interstices between the fibres induced a rapid increase in airflow resistance and therefore in filter pressure drop. During this stage, Agranovski and Braddock (1998) noted that part of the collected liquid migrates to downstream layers. When the change in liquid distribution is finished and liquid bridges are formed on most of the surface of the filter, drainage appears and the pressure drop becomes constant. A steady state is established among collection, re-entrainment and drainage of liquid droplets (Walsh et al., 1996).

All previous conclusions are based on observations of 2D surface photographs obtained by scanning electron microscopy (SEM). This apparatus allows only visualization of the filter surface instead of the complex three-dimensional structure in its depth. Therefore, it is classically assumed that deposits are the same in surface and in depth. Moreover, these results can be modified during the sample preparation because the structure can be damaged during the cutting step. The lack of understanding in liquid aerosol filtration, and particularly the few models of clogging in the literature partly result from the unavailability of tools to visualize and characterize the 3D porous filter properties and the spatial repartition of collected particles. Traditionally, methods such as mercury

intrusion porosimetry (Moscou and Lub, 1981) and liquid permeability (Robertson and Mason, 1949; Mason, 1950) have been used to characterize porous media. Nevertheless, these invasive techniques can estimate global structural properties of porous materials such as pore size distribution and global porosity but cannot give spatial information on the structure at the fibrous scale. Moreover, it is clear that these techniques are not suitable for samples containing a liquid.

X-ray microtomography may overcome the limitations of traditional 2D techniques and will enhance the understanding of filtration processes. For example, Lin and Miller (2000a, 2000b) used this technique for the characterization of the porous structure of a filter cake (with a voxel size of 17  $\mu\text{m}$ ) and Li et al. (2006) used X-ray microtomography for the observation of microsphere (36  $\mu\text{m}$  in size) deposition in granular beds (with a spatial resolution of 20  $\mu\text{m}$ ). To the best of our knowledge, X-ray microtomography has not been used to directly measure the actual distribution of liquid as a function of position in the medium at steady state. Bitten and Fochtman (1971) tried to measure this local distribution by joining different layers of filter media together. This study indicated a heterogeneous distribution of water in a glass–fibre coalescent filter and a liquid concentration 3–6 times greater at the inlet of the filter than in the rest of the medium. Andan et al. (2008) recently developed a theoretical model to investigate how the liquid saturation profile could affect the filter pressure drop and efficiency. However, given the lack of experimental results on the liquid distribution, saturation is modelled as linearly varying with the filter depth. In our study, synchrotron X-ray microtomography, which is a non-intrusive technique, was carried out to provide information about the three-dimensional structure of a porous medium and consequently the three-dimensional distribution of liquid in a clogged filter. The results can then be an input for the simulations in order to influence the influence of an unknown microscopic structure (Hyv aluoma et al., 2006).

## 2. Materials and methods

### 2.1. Synchrotron X-ray microtomography

Synchrotron X-ray microtomography is an outstanding method to investigate pore-scale processes at the micron level because it can produce information of the internal structure of samples (a review of applications is given by Moreno-Atanasio et al., 2010). In X-ray microtomography, the X-ray attenuation coefficient is studied and it was assumed that this attenuation is mainly due to absorption. This method overcomes the limitations of traditional two-dimensional imaging tools by providing higher quality data in term of signal to noise ratio and a high spatial resolution compared with classical laboratory equipments. This is due to the fact that synchrotron beams are tunable in terms of energy and size and are characterized by a high flux of photons. The data presented in this work were acquired on the ID 19 beam line of the European Synchrotron Radiation Facility (ESRF) located in Grenoble, France.

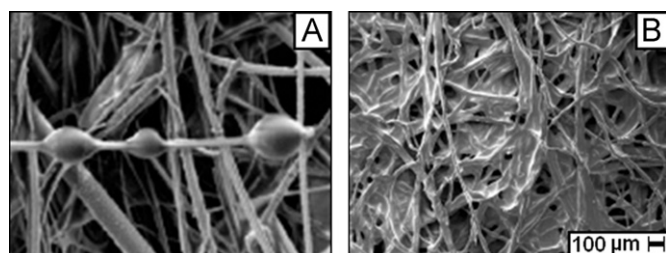


Fig. 1. SEM images of liquid deposits at different stages of filter clogging: (A) droplets on fibre surface (Contal et al., 2004) and (B) liquid bridges and films (Charvet et al., 2010).

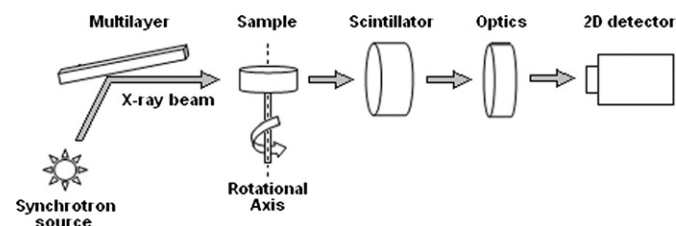
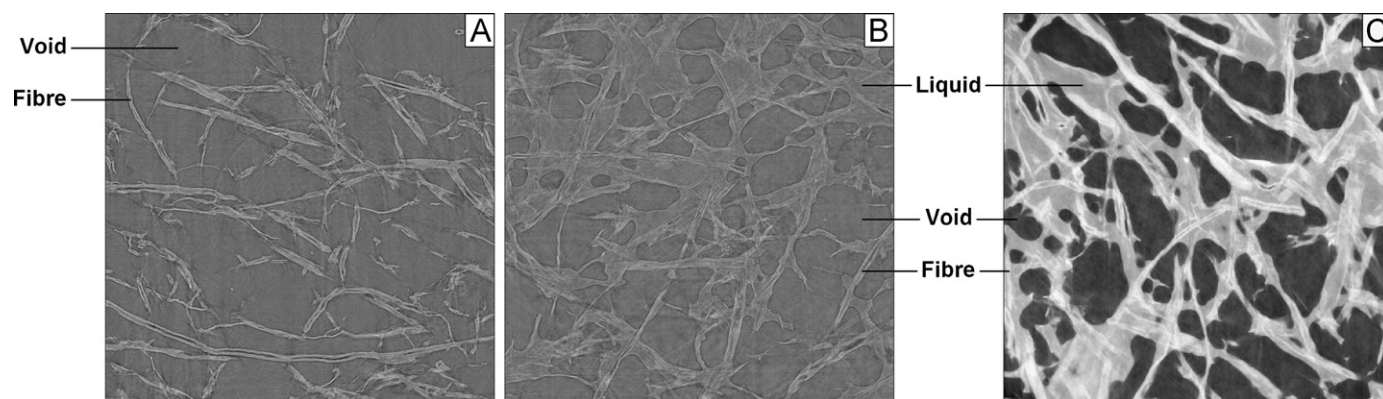


Fig. 2. Schematic view of the experimental set-up.



**Fig. 3.** Reconstructed images before denoising: (A) blank filter (tomography), (B) filter clogged with a liquid aerosol (tomography) and (C) filter clogged with a liquid aerosol (holotomography); European Synchrotron Radiation Facility, Grenoble, France;  $1050 \mu\text{m} \times 1050 \mu\text{m}$ .

A schematic view of the ID 19 experimental set-up is shown in Fig. 2. Rather than rotating the X-ray source and detectors during data collection, as in medical computerized tomography technology, the sample, fixed for example on a capillary tube, is set on the rotation stage. A parallel and monochromatic X-ray beam irradiates the sample. The transmitted beam is converted into visible light by a scintillator and the signal is then recorded with a Fast Read-Out Low-Noise camera (Labiche et al., 2007). The transmitted beam is classically recorded for about 1500 different angular positions equally spaced between  $0^\circ$  and  $180^\circ$ . The measuring time of this scan is less than 10 minutes. As these projections are known for a large number of angular orientations of the sample, it is possible, using a filter back projection algorithm, to quantitatively map the distribution of the X-ray absorption coefficient, which is displayed here in grey levels. To increase the contrast between liquid and fibrous phases and obtain a more robust reconstruction (Cloetens et al., 1999), we decided to conduct another experiment and to use quantitative phase tomography, also called holotomography. This method is based on the same principle as the microtomography. Instead of determining the linear attenuation coefficient at any point of the sample, for a given distance, the sample must be scanned several times (2–4) with various distances between it and the transmitted X-ray detector. Then, by combining these images taken at different distances from the sample, it is possible to obtain a quantitative three-dimensional mapping of the electron density. Recent developments allow the application of this technique to absorbent samples (Langer et al., 2010) such as clogged filters.

## 2.2. Sample preparation

The filter studied contains cellulose fibres and was clogged with a poly-dispersed liquid aerosol of di-ethyl-hexyl-sebacate (DEHS). During filter clogging, the filtration velocity and the DEHS concentration were maintained constant at  $21 \text{ cm s}^{-1}$  and  $200 \text{ mg m}^{-3}$ , respectively. The filters are 100 mm in diameter. The filtration was stopped when a steady state was established among collection, re-entrainment and drainage of liquid droplets, i.e. when a drainage was visible downstream of the filter. For more information on clogging, the experimental set-up is described in a previous article (Charvet et al., 2010). The clogged filter and the blank filter were then cut on a cutting table to obtain 2-mm/side samples. This cutting step can potentially damage the fibres on the sample edges. Consequently, these samples were deliberately larger than the area analysed by microtomography. Thus, the analysis, which takes place at the centre of the sample, is not affected by possible deterioration of the medium structure.

Environmental parameters (temperature and humidity) may be different in the storage room and in the experimental set-up room. Consequently, the filter structure may evolve during experiments because of its sensitivity to these parameters and the sample may swell during the data acquisition. Any structural changes during data acquisition lead to blurred data. The solution chosen to avoid this problem was to store samples in the experimental set-up room in advance (Rolland du Roscoat et al., 2005). Moreover, two samples taken from the same clogged filter were analysed 2 months apart. Data similarity suggests that the samples were well preserved over time.

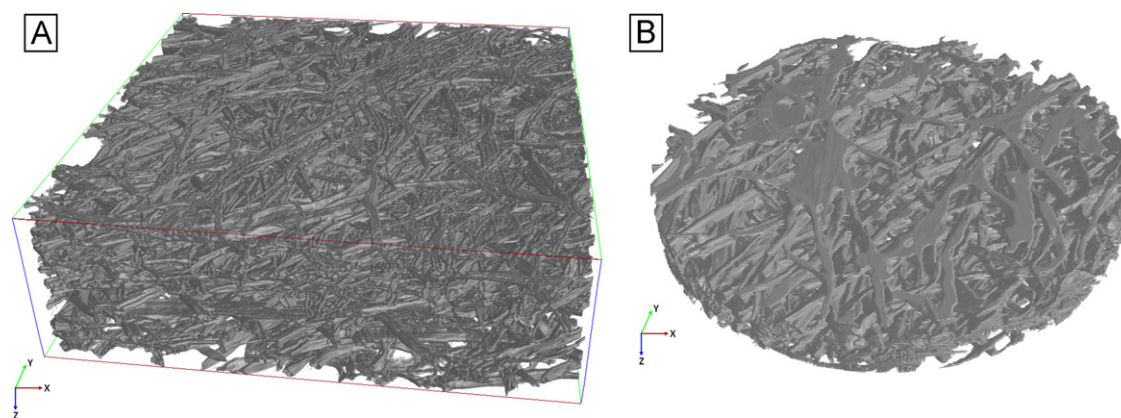
## 2.3. Image analysis

Fig. 3 shows reconstructed slices of the blank filter and the medium clogged with the liquid aerosol. These images are located approximately in the middle of the filter thickness and represent regions of interest ( $1500 \times 1500$  pixels) of the entire images ( $2048 \times 2048$  pixels). A  $0.7 \mu\text{m}$  pixel size was chosen in our experiments, providing a field of interest of  $1050 \mu\text{m} \times 1050 \mu\text{m} \times$  filter thickness. It has been proved that this volume is a representative elementary volume (REV), that means, it is sufficient to be the representative of the macroscopic characteristics of the filter (Rolland du Roscoat et al., 2007). The data show that the chosen voxel<sup>2</sup> size ( $0.7 \mu\text{m} \times 0.7 \mu\text{m} \times 0.7 \mu\text{m}$ ) is appropriate to visualize the different filter constituents. Other techniques such as magnetic resonance imaging (MRI) were used to determine the particle deposition in a fibrous filter (Hoferer et al., 2006). However, the resolution ( $235 \mu\text{m}$ ) and measuring time (4 hours) of this technique were not compatible with our aims.

On these 2D images extracted from the filter bulk, the porous phase and the solid phase (fibres) can be observed and in Fig. 3B and C, the liquid phase. The image sharpness shows the absence of oil movement during the scan. It can be noted that liquid and fibre phases present a similar absorption coefficient in Fig. 3B. It is therefore difficult to visualize the three phases using the tomography method. However, the aim of this investigation was to characterize the liquid distribution in a clogged filter. Consequently, fibres, stored liquid and void space must be separated. Hence, for the clogged filter, only the holotomography results, where the liquid and solid phases can be differentiated, will be discussed.

Three-dimensional visualizations (Fig. 4) are difficult to analyze due to the lack of clarity, but analysis of individual radiographs from

<sup>2</sup> A voxel is a three-dimensional pixel.



**Fig. 4.** Three-dimensional visualizations: (A) blank filter (tomography,  $1050\ \mu\text{m} \times 1050\ \mu\text{m} \times 350\ \mu\text{m}$ ) and (B) filter clogged with a liquid aerosol (holotomography,  $1450\ \mu\text{m} \times 1450\ \mu\text{m} \times 350\ \mu\text{m}$ ); European Synchrotron Radiation Facility, Grenoble, France.

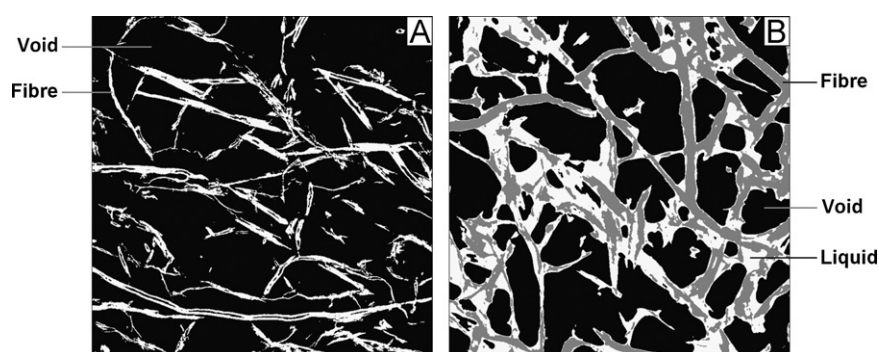


**Fig. 5.** Segmented and denoised images: (A) blank filter (tomography) and (B) filter clogged with a liquid aerosol (holotomography); European Synchrotron Radiation Facility, Grenoble, France;  $1050\ \mu\text{m} \times 1050\ \mu\text{m}$ .

synchrotron X-ray microtomography (Fig. 3B and C) highlights the formation of liquid menisci in the filter depth. These observations complete previous two-dimensional studies by scanning electron microscopy (SEM). Nevertheless, in order to determine the distribution of the liquid in the medium more precisely, X-ray microtomography images need to be segmented.

To calculate the porosity of samples, we need to separate the solid phase from the porous phase on grey images. This step, called segmentation, is a conversion process of a grey-scale image obtained from a tomography experiment, to a binary (for the blank filter) or a ternary image (for the clogged filter) by identifying different populations of pixels in the image. For a filter clogged with a liquid aerosol, these populations refer to the solid (fibres), gaseous (void space) and liquid phases, which are identified only with their different X-ray responses. The segmentation process is not precisely detailed here for the sake of simplicity (more information can be found in the article of Rolland du Roscoat et al., 2005). The results are presented in Fig. 5 for the blank filter and the medium clogged with a liquid aerosol. In these high-resolution images resulting from denoising and segmentation, black and white pixels represent, respectively, void space and fibres on Fig. 5A and black, grey and white pixels represent void space, fibrous and liquid phases, respectively, on Fig. 5B.

A Matlab code was developed to analyze the reconstructed and segmented images of the clogged filter. This analysis reveals the presence of pores on the sample boundaries, which are disconnected from others. However, this side effect is only due to the definition of the working area and therefore would logically disappear by reasoning on the entire filter. Moreover, some of the small closed pores, which appeared during the three-

dimensional treatment may come from segmentation uncertainty. Clogging the filter with a liquid aerosol does not seem to create closed pores that would increase the medium pressure drop significantly. Consequently, the increase in the pressure drop results from an increase in packing density (due to the mass of liquid collected), which will also cause changes in the three-dimensional structure and the filter's collection efficiency.

### 3. Results and discussion

#### 3.1. Qualitative analysis of the blank filter's three-dimensional structure

The filter packing density before clogging can be evaluated from segmented images of the clogged filter as the ratio of the pixels belonging to the fibrous phase (grey pixels) to the whole number of pixels on the surface of each image. Fig. 6 represents the porosity profiles, which have been calculated along the sample thickness (i.e. in the direction of the flow) and along the orthogonal directions normal to the flow (directions 1 and 2). This figure shows that the packing density is not constant throughout the thickness of the medium (black curve). This result is similar to those already measured in other porous materials such as papers (Rolland du Roscoat et al., 2007) and composites (Le et al., 2008). In the first layers of the blank filter, the presence of a strong gradient can be observed. These first slices account for about 7% of the total number of slices and are located on the upstream side of the filter during the filtration process. This porosity decrease is not only due to a porosity gradient on the edges of the filter but also to the samples'

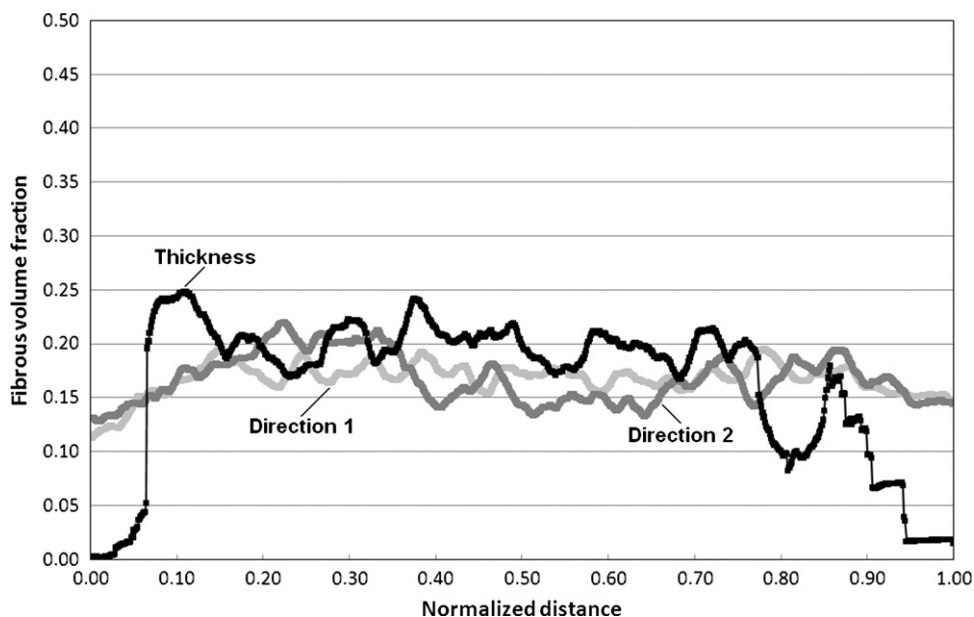


Fig. 6. Fibrous volume fraction along the three axes of the blank filter. The directions 1 and 2 correspond to the two orthogonal directions normal to the flow.

imperfect horizontal position. Indeed, the top and the bottom surfaces were not completely flat during the sample put in place or may have been slightly inclined with respect to the z-axis during the sample rotation stage. Consequently, because of this inclination, the first layers are not entirely covered by fibres and have a measured packing density lower than the actual packing density.

The same phenomenon was observed in the last layers (about 23% of the total slice number). The fibrous volume fraction between these two boundary effects is relatively constant. So, the initial porosity is quite homogeneous in the three dimensions of the filter volume. The packing densities obtained by holotomography were 0.20, 0.17 and 0.17 in the filter thickness and in the two orthogonal directions normal to the flow, respectively. The deviation between the fibrous volume fraction along the filter thickness and the two other packing densities can be explained by the difficulty in estimating the beginning and the end of the filter. Moreover, in order to test the reproducibility of the measurement, classical tomography images of the blank filter were analysed. The results of the fibrous volume fraction in the medium thickness (0.18) were close to those obtained by holotomography.

Nevertheless, the packing density obtained in the bulk of the medium slightly underestimates the measured one (about 0.27). The experimental packing density is obtained by weighing a given filter volume and by using the density of cellulose ( $1500 \text{ kg m}^{-3}$ ). The differences can be explained by the segmentation process during which the threshold that separates materials is determined. Indeed, the voxels are considered to belong to a phase (porous and fibrous) if their grey level passes a certain threshold. However, this threshold selection is somewhat arbitrary and therefore could incur uncertainties or errors by assigning voxels to an inappropriate phase.

Moreover, if we overcome the two boundary effects, the blank filter thickness can be calculated and compared with those obtained using other standard methods. The evaluation of the thickness ( $\mu\text{m}$ ),  $300 \pm 20$ ,  $330 \pm 30$  and  $340$  were obtained for Scanning Electron Microscopy, optical microscopy and the manufacturer's data, respectively. The filter thickness corresponds to about 500 slices of  $0.7 \mu\text{m}$  thickness. Hence, the thickness obtained with synchrotron X-ray microtomography data was about  $350 \mu\text{m}$ . Despite the difficulty in estimating the beginning and the end of the filter, the value obtained with microtomography data is close to the

thickness values given by the manufacturer and observed by optical microscopy and scanning electron microscopy.

### 3.2. Qualitative analysis of the clogged filter's three-dimensional structure

#### 3.2.1. Liquid distribution in the medium thickness

The volume fractions of void space, liquid and fibres were measured from the previous region of interest ( $1500 \times 1500$  pixels) perpendicular to the z-axis of the clogged filter and are presented in Fig. 7. The same phenomenon than in Fig. 6 can be observed in the first layers of the clogged filter. Indeed, the filter inclination tends to increase the porosity of the first and the last slices. Moreover, an increase in the fibrous volume fraction in the final layers can be noted. This observation results from the appearance of the capillary, which supports the sample (see the third image in Fig. 7). If we overcome these two boundary effects (filter inclination and capillary presence), the oil saturation evolves with filter thickness. The liquid volume fraction is quite constant in the first half of the clogged filter thickness, then it decreases and finally increases to a value close to 0.3. This final increase may be due to boundary effects and filter preparation. However, the results of this non-destructive technique are consistent with those of Bitten and Fochtman (1971), who reported a heterogeneous liquid distribution in a glass-fibre filter and a liquid concentration higher in the filter inlet than in the rest of the medium.

#### 3.2.2. Liquid distribution in the orthogonal directions normal to the flow

To determine the liquid distribution in the clogged filter more precisely, volume fractions were also calculated along the two orthogonal directions normal to the flow (Figs. 8 and 9). The liquid distribution seems to vary only in the thickness of the filter (Fig. 7) and not in the directions normal to the flow. The porous volume fraction of the entire clogged filter obtained by analysis of holotomography images is about 60%, whereas it is close to 20% for the experimental analysis (as for the blank filter analysis, the experimental porosity is obtained by weighing a given volume of the filter and using densities of cellulose and oil). This difference can be explained with the horizontal position of the medium during

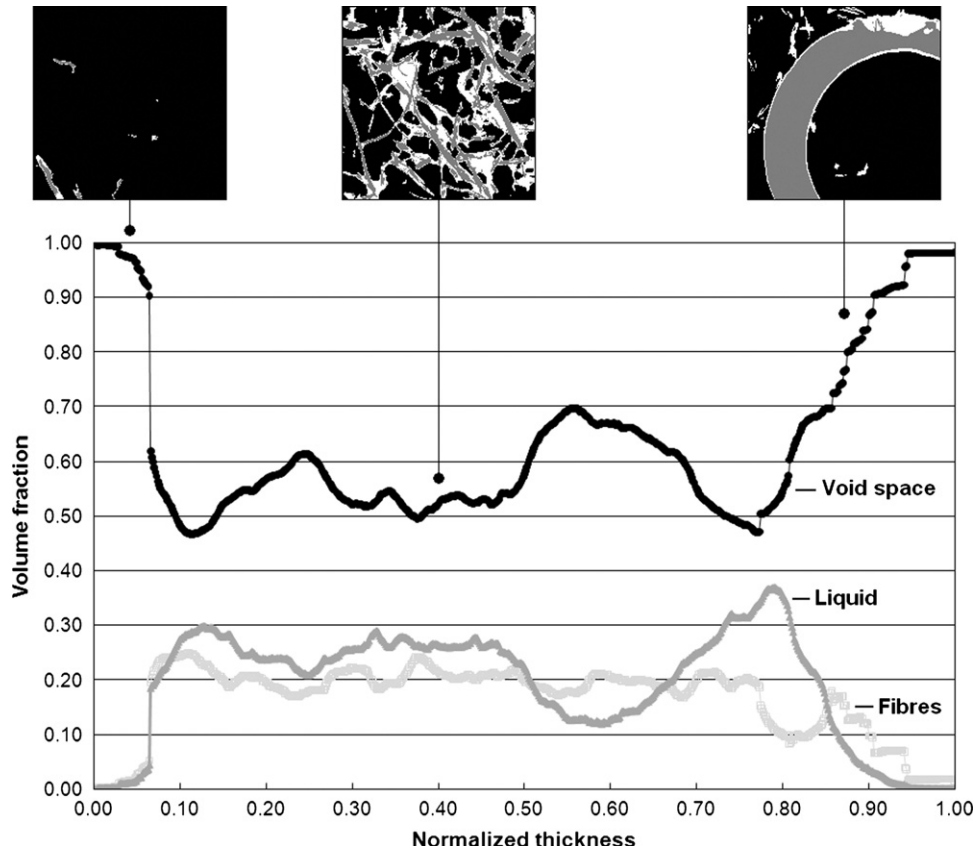


Fig. 7. Volume fraction of the different phases and segmented images along the normalized thickness of the filter clogged with a liquid aerosol.

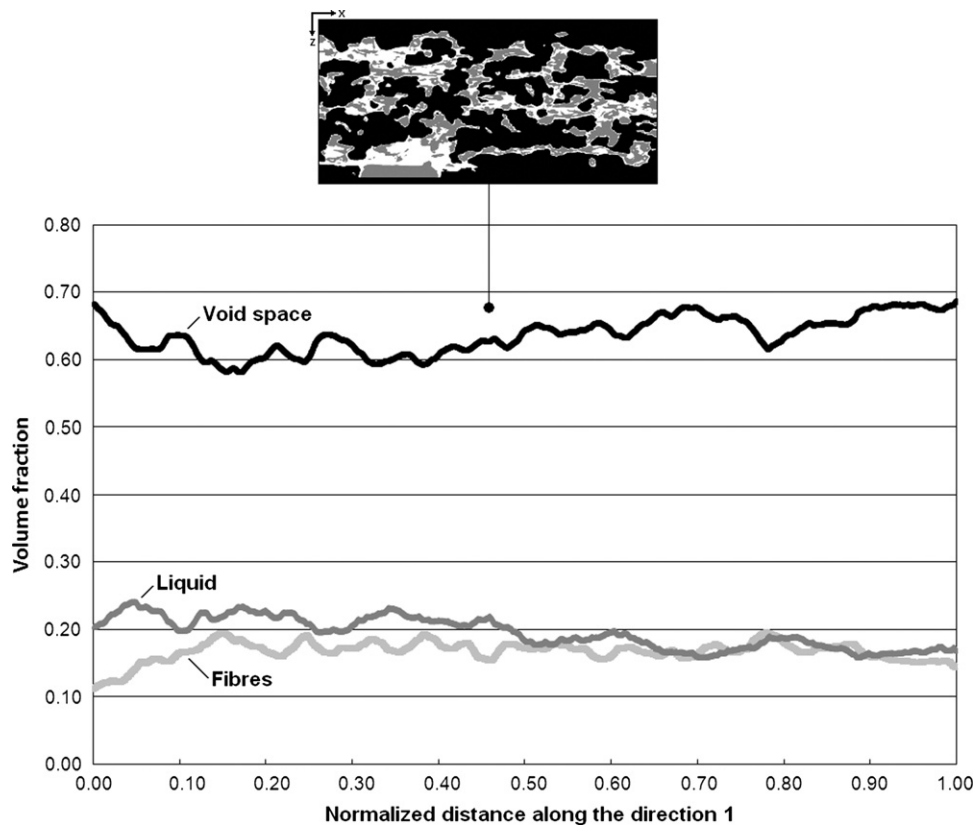


Fig. 8. Volume fraction of the different phases of the clogged filter along a direction normal to the flow (direction 1).

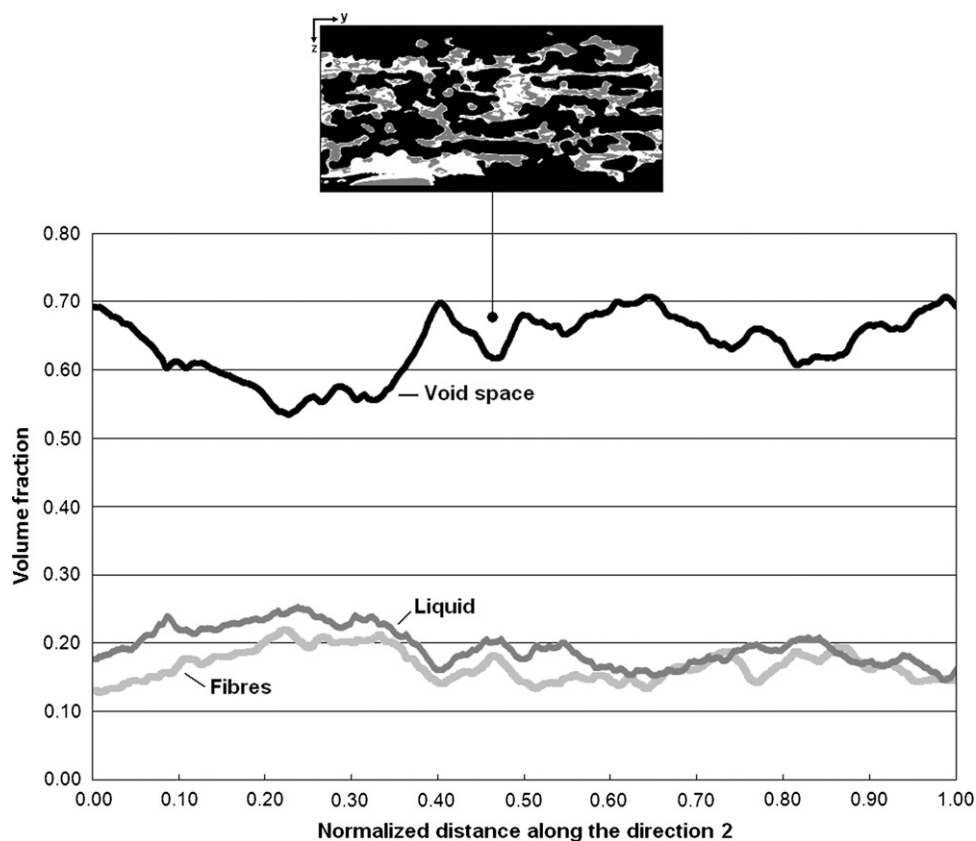


Fig. 9. Volume fraction of the different phases of the clogged filter along a direction normal to the flow (direction 2).

the filtration process (Charvet et al., 2010). Because of this horizontal position of the medium, there is an accumulation of liquid on the upper and lower sides of the filter during the drainage stage. Therefore, the calculation (by weighing) of the experimental porous volume fraction is distorted. Indeed, this liquid is considered to be trapped in the filter and thus enhanced the filter packing density. Consequently, experimental calculation gives the values far higher than the true packing density and than the liquid volume fraction obtained by microtomography.

#### 4. Conclusion

Until now, observations of clogged fibrous filters have been made by scanning electron microscopy and various authors have demonstrated the formation of liquid menisci on the medium's upstream surface during the filtration of liquid aerosols. The use of synchrotron X-ray holotomography and the resulting image analyses have made it possible to complete these studies and also to highlight the formation of liquid menisci in the filter depth.

The analysis of the volume fraction of the clogged filter has also highlighted a heterogeneous liquid distribution. The liquid volume fraction is higher in the first layers of the clogged filter and therefore a larger quantity of liquid is trapped in the upstream layers of the medium. In order to confirm these results, samples at different clogging stages and varying operating conditions (filtration velocity, DEHS concentration) must be analysed by synchrotron X-ray microtomography. Moreover, these results probably do not provide the actual liquid distribution during filtration because a slight redistribution must occur due to the discontinuation of gas flow. Indeed, it is necessary to stop the kinetic to make a measurement and this problem also occurs during image acquisition by scanning electron microscopy. Nevertheless, the real-time

measurements (during filter clogging) with microtomography seem difficult to set due to the time required to scan a 3D sample.

Furthermore, highlighting the presence of menisci confirms that the liquid does not form films on the fibre surface and therefore that the fibre diameter must be considered as a constant when modelling filter clogging. Moreover, the heterogeneous liquid distribution along the filter thickness encourages us not to consider the entire filter as homogeneous and therefore to discretize the medium when modelling and to consider different characteristics (packing density and interstitial velocity) for each theoretical slice. Therefore, the present study can provide valuable information, especially for efficiency and pressure drop modelling during filter clogging by a liquid aerosol.

#### Acknowledgments

The authors would like to thank ESRF for its scientific support throughout the ma127 "Heterogeneous fibrous materials" project.

#### References

- Agranovski, I.E., Braddock, R.D., 1998. Filtration of liquid aerosols on wettable fibrous filters. *AIChE Journal* 44, 2775–2783.
- Andan, S., Hariharan, S.I., Chase, G.G., 2008. Continuum model evaluation of the effect of saturation on coalescence filtration. *Separation Science and Technology* 43, 1955–1973.
- Bitten, J.F., Fochtman, E.G., 1971. Water distribution in fiber-bed coalescers. *Journal of Colloid and Interface Science* 37, 312–317.
- Boundy, M., Leith, D., David, H., Michael, G., Edward, B.G., 2000. Performance of industrial mist collectors over time. *Applied Occupational and Environmental Hygiene* 15, 928–935.
- Brink, J.A., Burggrabe, W.F., Greenwell, L.E., 1966. Mist removal from compressed air. *Chemical Engineering Progress* 62, 60–65.

- Charvet, A., Gonthier, Y., Bernis, A., Gonze, E., 2008. Filtration of liquid aerosols with a horizontal fibrous filter. *Chemical Engineering Research and Design* 86, 569–576.
- Charvet, A., Gonthier, Y., Gonze, E., Bernis, A., 2010. Experimental and modelled efficiencies during the filtration of a liquid aerosol with a fibrous medium. *Chemical Engineering Science* 65, 1875–1886.
- Cloetens, P., Ludwig, W., Baruchel, J., Van Dyck, D., Van Landuyt, J., Guigay, J.P., Schlenker, M., 1999. Holotomography: quantitative phase tomography with micrometer resolution using hard synchrotron radiation X-rays. *Applied Physics Letters* 75, 2912–2914.
- Contal, P., Simao, J., Thomas, D., Frising, T., Callé, S., Appert-Collin, J.C., Bemer, D., 2004. Clogging of fibre filters by submicron droplets—phenomena and influence of operating conditions. *Journal of Aerosol Science* 35, 263–278.
- Cooper, S.J., Leith, D., 1998. Evaporation of metalworking fluid mist in laboratory and industrial mist collectors. *American Industrial Hygiene Association Journal* 59, 45–51.
- Frising, T., Thomas, D., Bemer, D., Contal, P., 2005. Clogging of fibrous filters by liquid aerosol particles: experimental and phenomenological modelling study. *Chemical Engineering Science* 60, 2751–2762.
- Gougeon, R., 1994. Filtration des aérosols liquides par les filtres à fibres en régimes d'interception et d'inertie, PhD Thesis (in French), University of Paris-Val-de-Marne, Paris, France.
- Gunter, K.L., Sutherland, J.W., 1999. An experimental investigation into the effect of process conditions on the mass concentration of cutting fluid mist in turning. *Journal of Cleaner Production* 7, 341–350.
- Hoferer, J., Lehmann, M.J., Hardy, E.H., Meyer, J., Kasper, G., 2006. Highly resolved determination of structure and particle deposition in fibrous filters by MRI. *Chemical Engineering & Technology* 29, 816–819.
- Hyväluoma, J., Raiskinmäki, P., Jäsberg, A., Koponen, A., Kataja, M., Timonen, J., 2006. Simulation of liquid penetration in paper. *Physical Review E—Statistical, Nonlinear, and Soft Matter Physics* 73, 1–8.
- Labiche, J.-C., Mathon, O., Pascarelli, S., Newton, M.A., Ferre, G.G., Curfs, C., Vaughan, G., Carreiras, D.F., 2007. Invited article: the fast readout low noise camera as a versatile X-ray detector for time resolved dispersive extended X-ray absorption fine structure and diffraction studies of dynamic problems in materials science, chemistry, and catalysis. *Review of Scientific Instruments* 78, 91301–91312.
- Langer, M., Cloetens, P., Peyrin, F., 2010. Regularization of phase retrieval with phase-attenuation duality prior for 3D holotomography. *IEEE Transactions on Image Processing* 19, 2428–2436.
- Le, T.-H., Dumont, P.J.J., Orgéas, L., Favier, D., Salvo, L., Boller, E., 2008. X-ray phase contrast microtomography for the analysis of the fibrous microstructure of SMC composites. *Composites Part A: Applied Science and Manufacturing* 39, 91–103.
- Liew, T.P., Conder, J.R., 1985. Fine mist filtration by wet filters—I. Liquid saturation and flow resistance of fibrous filter. *Journal of Aerosol Science* 16, 497–509.
- Li, X., Lin, C.L., Miller, J.D., Johnson, W.P., 2006. Pore-scale observation of microsphere deposition at grain-to-grain contacts over assemblage-scale porous media domains using X-ray microtomography. *Environmental Science and Technology* 40, 3762–3768.
- Lin, C.L., Miller, J.D., 2000a. Network analysis of filter cake pore structure by high resolution X-ray microtomography. *Chemical Engineering Journal* 77, 79–86.
- Lin, C.L., Miller, J.D., 2000b. Pore structure and network analysis of filter cake. *Chemical Engineering Journal* 80, 221–231.
- Mason, S.G., 1950. The specific surface of fibers—its measurement and application. *Tappi Journal* 33, 403–409.
- Moreno-Atanasio, R., Williams, R.A., Jia, X., 2010. Combining X-ray microtomography with computer simulation for analysis of granular and porous materials. *Particuology* 8, 81–99.
- Moscou, L., Lub, S., 1981. Practical use of mercury porosimetry in the study of porous solids. *Powder Technology* 29, 45–52.
- Mullins, B.J., Kasper, G., 2006. Comment on “Clogging of fibrous filters by liquid aerosol particles—experimental and phenomenological modelling study” by Frising et al. *Chemical Engineering Science* 61, 6223–6227.
- Robertson, A.A., Mason, S.G., 1949. Specific surface of cellulose fibers by the liquid permeability method. *Pulp Paper Magazine Canada* 50, 103–110.
- Rolland du Roscoat, S., Bloch, J.-F., Thibault, X., 2005. Synchrotron radiation microtomography applied to investigation of paper. *Journal of Physics D: Applied Physics* 38, A78–A84.
- Rolland du Roscoat, S., Decain, M., Thibault, X., Geintreau, C., Bloch, J.-F., 2007. Estimation of microstructural properties from synchrotron X-ray microtomography and determination of the REV in paper materials. *Acta Materialia* 55, 2841–2850.
- Simpson, A.T., Groves, J.A., Unwin, J., Piney, M., 2000. Mineral oil metal working fluids (MWFs)—development of practical criteria for mist sampling. *The Annals of Occupational Hygiene* 44, 165–172.
- Tekasakul, S., Suwanwong, P., Otani, Y., Tekasakul, P., 2008. Pressure drop evolution of a medium-performance fibrous filter during loading of mist aerosol particles. *Aerosol and Air Quality Research* 8, 348–365.
- Thornburg, J., Leith, D., 2000. Size distribution of mist generated during metal machining. *Applied Occupational and Environmental Hygiene* 15, 618–628.
- Walsh, D.C., Stenhouse, J.I.T., Scurrah, K.L., Graef, A., 1996. The effect of solid and liquid aerosol particle loading on fibrous filter material performance. *Journal of Aerosol Science* 27, 617–618.